



## Effects of alkyl chains on intermolecular packing and device performance in small molecule based organic solar cells



Yamin Zhang<sup>a, b</sup>, Miaomiao Li<sup>a, b</sup>, Huanran Feng<sup>a, b</sup>, Wang Ni<sup>a, b</sup>, Hongtao Zhang<sup>a, b</sup>, Feng Liu<sup>c</sup>, Xiangjian Wan<sup>a, b</sup>, Yongsheng Chen<sup>a, b, \*</sup>

<sup>a</sup> The Centre of Nanoscale Science and Technology and Key Laboratory of Functional Polymer Materials, State Key Laboratory and Institute of Elemento-Organic Chemistry, Collaborative Innovation Center of Chemical Science and Engineering (Tianjin), College of Chemistry, Nankai University, Tianjin, 300071, China

<sup>b</sup> School of Materials Science and Engineering, The National Institute for Advanced Materials, Nankai University, Tianjin, 300071, China

<sup>c</sup> Department of Physics and Astronomy, Shanghai Jiao Tong University, Shanghai, 200240, China

### ARTICLE INFO

#### Article history:

Received 18 December 2016

Received in revised form

10 February 2017

Accepted 11 February 2017

Available online 17 February 2017

#### Keywords:

Alkyl chain

Core unit

Intermolecular packing

Organic solar cell

### ABSTRACT

Two donor molecules named as DR3TDTC-C6 and DR3TDTC-C8 with n-hexyl and n-octyl alkyl chains on the central building block 7H-cyclopenta-[1,2-*b*:3,4-*b'*]-dithiophene (DTC) were designed and synthesized. Both of them exhibited PCEs >4%. The photovoltaic properties of these molecules were superior to their analogous donor molecule DR3TDTC, which possess two 2-ethyl hexyl alkyl chains on the same core unit and only demonstrated a PCE of 0.75% after elaborative post-treatment. The influence of the alkyl chains on the optical, electrochemical properties, packing properties and morphology of these three molecules was systematically investigated. The results demonstrated that the difference between their device performances is mainly affected by their intermolecular packing state. This indicates that length and branch structure of alkyl chains on the central unit should be given careful consideration while designing donor molecules for small molecular organic solar cells.

© 2017 Elsevier Ltd. All rights reserved.

## 1. Introduction

Organic photovoltaics (OPVs), on account of their flexibility, low cost, light weight and solution processability, have been considered to be one of promising candidates to solve the worldwide energy problem [1–8]. In the past two decades, power conversion efficiencies (PCEs) over 10% for single cells and over 11% for tandem devices have been achieved for polymer-based OPVs (P-OPVs) with the bulk hetero junction (BHJ) architecture [9–21]. Small molecule based OPVs (SM-OPVs), as a competitive alternative to their polymer counterparts, have also demonstrated PCEs exceeding 10% for single cells soon afterwards [22–24]. Lately, PCE over 12% has been achieved by solution-processed tandem solar cell based on the small molecules [25]. It is worthy to note that SM-OPVs own several

peculiar advantages, such as defined structures without batch-to-batch variations, easy control of energy levels by chemical structure designing, and relatively simple synthesis and purification, demonstrating that SM-OPVs exhibit great potential for OPV technologies [26–29].

In recent years, small molecule donors with electron acceptor–donor–acceptor (A–D–A) architecture conjugated framework have shown great success and PCE over 10% have been achieved [27,30–35]. These molecules are consisted of four parts: donor/acceptor (D/A) units, conjugated bridges, substituent groups and side chains. For these A–D–A type molecule design, much more attentions have been drawn on the D–A units and conjugated bridges [36]. In fact, side-chains also play great roles on the molecules physical properties and corresponding device performances. Generally, side chains can not only increase solubility but also tune the intermolecular packing state and thus influence the hole mobility, absorption spectra, electronic energy levels and the final photovoltaic performance. Some results have already indicated that even a subtle change of the flexible chains could result in a great influence on device performance. For example, Kim et al. reported three small molecules with different alkyl side chains (n-octyl, n-

\* Corresponding author. The Centre of Nanoscale Science and Technology and Key Laboratory of Functional Polymer Materials, State Key Laboratory and Institute of Elemento-Organic Chemistry, Collaborative Innovation Center of Chemical Science and Engineering (Tianjin), College of Chemistry, Nankai University, Tianjin, 300071, China.

E-mail address: [yschen99@nankai.edu.cn](mailto:yschen99@nankai.edu.cn) (Y. Chen).

decyl, and 2-ethylhexyl chains) on the thiophene conjugated bridges and successfully controlled their intermolecular distance through this side chain engineering [37]. Our group reported that the alkyls chains on the terminal groups could not only influence on the small molecules solubilities but also change their packing behaviors and solid-state miscibility with fullerene derivatives [38]. In contrast, less attentions have been drawn on the influence of alkyl chains of the central building blocks for these A-D-A types small molecular donor materials [39].

In our previous work, a small molecule donor material named DR3TDTC with two 2-ethylhexyl side chains on the central unit 7H-cyclopenta-[1,2-*b*:3,4-*b'*]-dithiophene (DTC) has been synthesized. Devices based on DR3TDTC:PC<sub>71</sub>BM blend films exhibited a poor PCE of 0.75% [40]. Considering the side chains' significant effects, we herein reported two molecules named DR3TDTC-C6 and DR3TDTC-C8 (Scheme 1), which have the same backbone structure with DR3TDTC but different alkyls chains on the central DTC block. Our goal is to gain a deep understanding of the central building blocks alkyls chains effects on the intermolecular packing and blend morphology as well as their performance in photovoltaic devices.

## 2. Materials and methods

### 2.1. Materials

All reactions and manipulations were carried under an argon atmosphere using standard Schlenk techniques [6,6]-Phenyl-C<sub>71</sub>-butyric acid methyl ester (PC<sub>71</sub>BM) was purchased from American Dye Source, Inc. Other starting materials were all purchased from commercial suppliers and used without further purification unless otherwise noticed.

### 2.2. Instruments and measurements

The <sup>1</sup>H nuclear magnetic resonance (NMR) spectra were taken on a Bruker AV400 Spectrometer. Matrix assisted laser desorption/ionization time-of-flight mass spectrometry (MALDI-TOF MS) was performed on a BrukerAutoflex III instrument. Transmission electron microscopy (TEM) was performed on a Philips Technical G2F20 at 200 kV. Thermogravimetric analysis (TGA) were carried out on a NETZSCH STA 409PC instrument under a purified nitrogen gas flow with a 10 °C min<sup>-1</sup> heating rate. UV–vis spectra were obtained with a JASCO V-570 spectrophotometer. Cyclic voltammetry (CV) experiments were performed with a LK2010 in dichloromethane solutions (GP). All measurements were carried out at room temperature with a conventional three-electrode configuration using a glassy carbon electrode as the working electrode, a saturated calomel electrode (SCE) as the reference electrode, and a Pt wire as the counter electrode. Tetrabutyl ammonium phosphorus

hexafluoride (Bu<sub>4</sub>NPF<sub>6</sub>, 0.1 M) in dichloromethane was used as the supporting electrolyte, and the scan rate was 100 mV s<sup>-1</sup>.

The current density–voltage (J–V) characteristics of photovoltaic devices were obtained by a Keithley 2400 source-measure unit. The photocurrent was measured under simulated illumination of 100 mW cm<sup>-2</sup> with AM 1.5G irradiation using a xenon-lamp-based solar simulator [Oriel 96000 (AM1.5G)] in an argon-filled glove box. Simulator irradiance was characterized using a calibrated spectrometer, and illumination intensity was set using a certified silicon diode. External quantum efficiency values (EQEs) of the encapsulated devices were obtained with a halogen-tungsten lamp, monochromator, optical chopper, and lock-in amplifier in air and the photon flux was determined by a calibrated silicon photodiode. Hole mobility was measured by space charge limited current (SCLC) method using a diode configuration of ITO/PEDOT:PSS/donor:PC<sub>71</sub>BM/Au by taking the dark current density in the range of 0–6 V and fitting the results to a space charge limited form, where SCLC is described by:

$$J = \frac{9\epsilon_0\epsilon_r\mu_0V^2}{8L^3} \exp\left(0.89\beta\sqrt{\frac{V}{L}}\right)$$

where J is the current density, L is the film thickness of the active layer,  $\mu_0$  is the hole or electron mobility,  $\epsilon_r$  is the relative dielectric constant of the transport medium,  $\epsilon_0$  is the permittivity of free space ( $8.85 \times 10^{-12}$  F m<sup>-1</sup>), V (=V<sub>appl</sub> - V<sub>bi</sub>) is the internal voltage in the device, where V<sub>appl</sub> is the applied voltage to the device and V<sub>bi</sub> is the built-in voltage due to the relative work function difference of the two electrodes.

### 2.3. Fabrication of organic solar cells

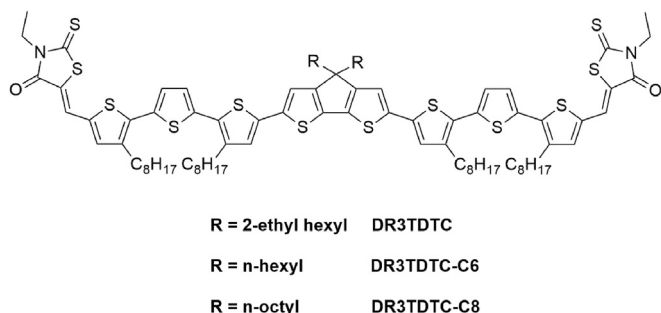
The photovoltaic devices were fabricated with a structure of glass/ITO/PEDOT:PSS/donor: acceptor/ETL-1/Al. ETL-1, used as the interfacial layer for cathode, is a methanol soluble fullerene surfactant developed by Alex K.-Y [41], and its structure is shown in Fig. S1. The ITO-coated glass substrates were cleaned by ultrasonic treatment in detergent, deionized water, acetone, and isopropyl alcohol under ultrasonic for 15 min each time and subsequently dried by a nitrogen flow. A thin layer of PEDOT:PSS (Baytron P VPAI 4083, filtered at 0.45  $\mu$ m) was spin-coated (3000 rpm, ca. 40 nm thick) onto the ITO surface. After baking at 150 °C for 20 min, the substrates were transferred into an argon-filled glove box. Subsequently, a donor: PC<sub>71</sub>BM blend solution in chloroform (1:0.8 w/w, 10 mg mL<sup>-1</sup> for donor component) was spin coated at 1700 rpm for 20 s on the ITO/PEDOT:PSS substrate. After the active layer spin coated, solvent vapor annealing was used to tune the blend film morphology. For solvent vapor annealing, the films were placed in a glass petridish which containing 150  $\mu$ L chloroform for 90 s. Subsequently, ETL-1 was spin-cast on top of the active layer. Finally, 80 nm Al layer was deposited on the ETL-1 film under high vacuum (<2  $\times 10^{-4}$  Pa). The thicknesses of the ETL-1 and active layers were measured using Dektak 150 profilometer. The effective area of each cell was 4 mm<sup>2</sup> as defined by masks.

### 2.4. Synthesis

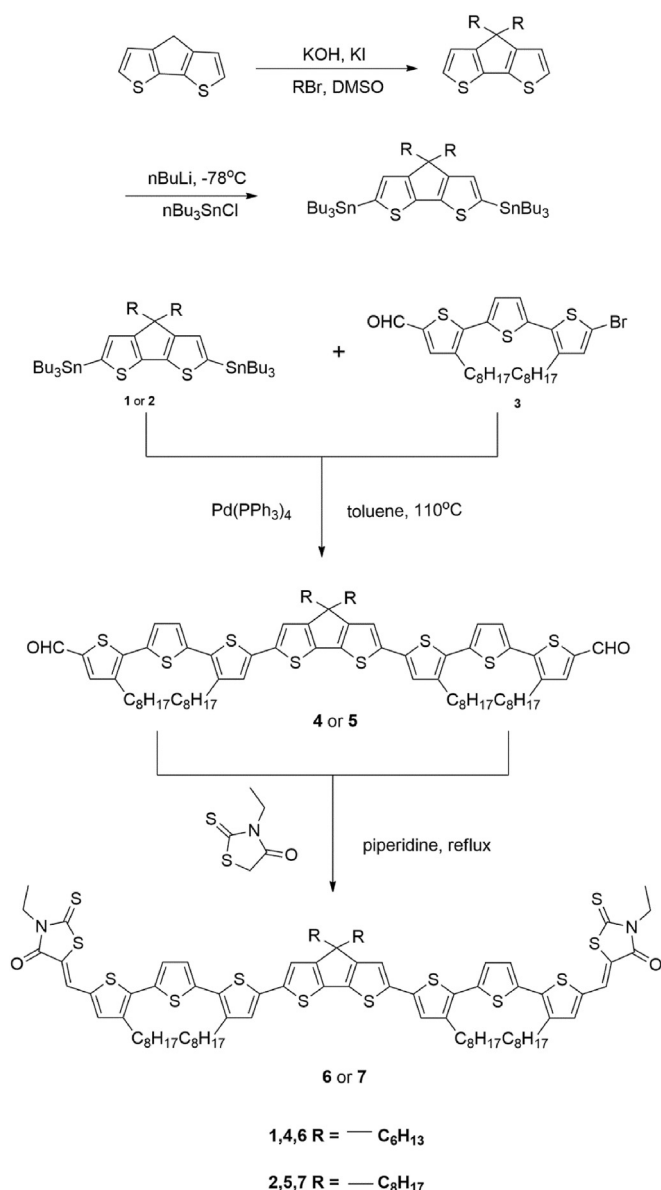
The synthesis routes of DR3TDTC-C8 and DR3TDTC-C6 are shown in Scheme 2. Compounds 1, 2, 3 were synthesized according to the literature [40,42,43].

#### 2.4.1. Synthesis of DCHO3TDTC-C6 (compound 4)

A solution of compounds 1 (2.66 g, 2.88 mmol) and 3 (3.51 g, 6.05 mmol) in dehydrated toluene (20 mL) was degassed twice



Scheme 1. Chemical structures of DR3TDTC, DR3TDTC-C6, DR3TDTC-C8.



**Scheme 2.** Synthesis route of DR3TDTC-C6 and DR3TDTC-C8.

with argon followed by the addition of Pd(PPh<sub>3</sub>)<sub>4</sub> (0.10 g, 0.087 mmol). After stirring at 100 °C for 24 h under argon, the reaction mixture was poured into cold water and extracted with CHCl<sub>3</sub>. The organic layer was washed with water and then dried over anhydrous Na<sub>2</sub>SO<sub>4</sub>. After removal of the solvent, the crude product was purified by silica gel using a mixture of dichloromethane and petroleum ether (2:1) as eluent to yield compound 4 (1.87 g, 48.5%). <sup>1</sup>H NMR (400 MHz, CDCl<sub>3</sub>): δ 9.83 (s, 2H), 7.60 (s, 2H), 7.25 (s, 2H), 7.12 (s, 2H), 7.04 (d, 4H), 2.84–2.78 (m, 8H), 1.86 (t, 4H), 1.71 (m, 8H), 1.42–1.17 (m, 56H), 0.89 (m, 18H). MS (MALDI-TOF): calcd for C<sub>79</sub>H<sub>106</sub>O<sub>2</sub>S<sub>8</sub> [M<sup>+</sup>], 1342.60; found: 1342.79.

#### 2.4.2. Synthesis of DCHO3TDTC-C8 (compound 5)

A solution of compounds 2 (2.43 g, 2.48 mmol) and 3 (3.02 g, 5.21 mmol) in dehydrated toluene (20 mL) was degassed twice with argon followed by the addition of Pd(PPh<sub>3</sub>)<sub>4</sub> (0.10 g, 0.087 mmol). After stirring at 100 °C for 24 h under argon, the reaction mixture was poured into cold water and extracted with CHCl<sub>3</sub>. The organic layer was washed with water and then dried over anhydrous

MgSO<sub>4</sub>. After removal of the solvent, the crude product was purified by silica gel using a mixture of dichloromethane and petroleum ether (2:1) as eluent to yield compound 5 (1.65 g, 47.6%). <sup>1</sup>H NMR (400 MHz, CDCl<sub>3</sub>): δ 9.83 (s, 2H), 7.60 (s, 2H), 7.25 (s, 2H), 7.12 (s, 2H), 7.04 (d, 4H), 2.84–2.78 (m, 8H), 1.86 (t, 4H), 1.71 (m, 8H), 1.42–1.17 (m, 64H), 0.89 (m, 18H). MS (MALDI-TOF): calcd for C<sub>83</sub>H<sub>114</sub>O<sub>2</sub>S<sub>8</sub> [M<sup>+</sup>], 1398.66; found: 1398.88.

#### 2.4.3. Synthesis of DR3TDTC-C6 (compound 6)

Compound 4 (258 mg, 0.19 mmol) and 3-ethyl-rhodanine (580 mg, 3.59 mmol) was dissolved in a solution of dehydrated chloroform (100 mL), then three drops of piperidine were added, the mixture was stirred overnight under argon at 70 °C. The solvent was then removed by a rotating evaporator and the crude product was dissolved in chloroform (10 mL), and then precipitated from methanol and the precipitate was filtered off. The residue was purified by silica gel chromatography using a mixture of petroleum ether and chloroform (1:4) as eluent and the crude solid was recrystallized from a hexane and chloroform mixture three times to produce DR3TDTC-C6 (188 mg, 60.7%). <sup>1</sup>H NMR (400 MHz, CDCl<sub>3</sub>): δ 7.79 (s, 2H), 7.26–7.03 (b, 10H), 4.20–4.18 (m, 4H), 2.83–2.78 (m, 8H), 1.86 (m, 4H), 1.71–1.68 (m, 8H), 1.56–1.40 (m, 12H), 1.31–1.17 (m, 44H), 1.02–1.01 (m, 6H), 0.88 (m, 18H). MS (MALDI-TOF): calcd for C<sub>89</sub>H<sub>116</sub>N<sub>2</sub>O<sub>2</sub>S<sub>12</sub> [M<sup>+</sup>], 1629.57; found: 1629.67.

#### 2.4.4. Synthesis of DR3TDTC-C8 (compound 7)

Compound 5 (249 mg, 0.18 mmol) and 3-ethyl-rhodanine (550 mg, 3.41 mmol) was dissolved in a solution of dehydrated chloroform (100 mL), then three drops of piperidine were added, and the mixture was stirred overnight under argon at 70 °C. The solvent was then removed by a rotating evaporator and the crude product was dissolved in chloroform (10 mL), and then precipitated from methanol and the precipitate was filtered off. The residue was purified by silica gel chromatography using a mixture of petroleum ether and chloroform (1:3) as eluent and the crude solid was recrystallized from a hexane and chloroform mixture three times to produce DR3TDTC-C8 (200 mg, 65.9%). <sup>1</sup>H NMR (400 MHz, CDCl<sub>3</sub>): δ 7.79 (s, 2H), 7.26–7.03 (b, 10H), 4.20–4.18 (m, 4H), 2.81–2.79 (m, 8H), 1.86 (m, 4H), 1.71–1.69 (m, 8H), 1.55–1.42 (m, 12H), 1.30–1.17 (m, 52H), 1.02–1.01 (m, 6H), 0.88 (m, 18H). MS (MALDI-TOF): calcd for C<sub>89</sub>H<sub>116</sub>N<sub>2</sub>O<sub>2</sub>S<sub>12</sub> [M<sup>+</sup>], 1685.63; found: 1685.92.

## 3. Results and discussion

### 3.1. Synthesis and thermal properties

As shown in Scheme 2, the intermediates of dialdehyde 4 and 5 were synthesized using Stille coupling, and the target molecules 6 and 7 were then prepared by Knoevenagel condensation of 4 or 5 with 3-ethyl-rhodanine. TGA indicates that DR3TDTC-C6 (compound 6) and DR3TDTC-C8 (compound 7) exhibit good thermal stability up to 300 °C under a N<sub>2</sub> atmosphere (see Fig. 1).

### 3.2. Optical properties and electrochemical properties

The UV–vis absorption spectra of DR3TDTC-C6 and DR3TDTC-C8 in a dilute chloroform solution and in the solid state are shown in Fig. 2 DR3TDTC-C6 in chloroform shows a maximum absorption peak at 532 nm with a maximum absorption coefficient of 7.96 × 10<sup>4</sup> M<sup>-1</sup> cm<sup>-1</sup>. In the solid state, a red shifted maximum absorption peak is observed at 624 nm for the DR3TDTC-C6 film. The DR3TDTC-C8 solution also shows a maximum absorption peak at 532 nm with absorption coefficient of 8.22 × 10<sup>4</sup> M<sup>-1</sup> cm<sup>-1</sup>. The film of DR3TDTC-C8 also shows similar red-shifted maximum absorption peak at 626 nm with DR3TDTC-C6. As shown in Fig. 2 and

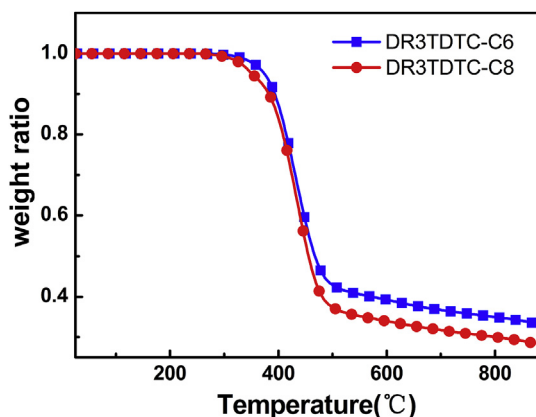


Fig. 1. Thermogravimetric analysis (TGA) plot of DR3TDTC-C6 and DR3TDTC-C8 with a heating rate of  $10\text{ }^{\circ}\text{C min}^{-1}$  under  $\text{N}_2$  atmosphere.

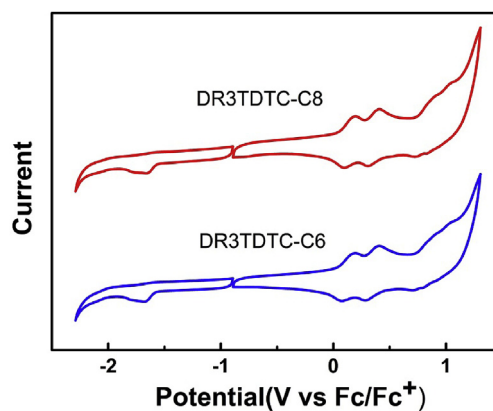


Fig. 3. Cyclic voltammetry (CV) of DR3TDTC-C6 and DR3TDTC-C8 in dichloromethane with  $0.1\text{ M Bu}_4\text{NPF}_6$ .

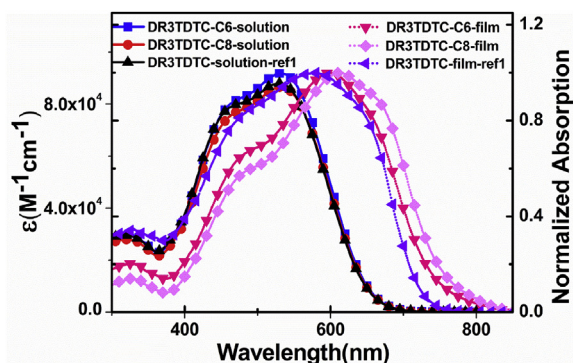


Fig. 2. UV-Vis absorption spectra of DR3TDTC-C6, DR3TDTC-C8 and DR3TDTC in chloroform solutions and as-cast films.

Table 1, both of DR3TDTC-C6 and DR3TDTC-C8 exhibited shifted absorption band than that of DR3TDTC in solid state, which could be attributed to the better intermolecular packing properties of these two new molecules.

The electrochemical properties of DR3TDTC-C6 and DR3TDTC-C8 were investigated by cyclic voltammetry (CV). Ferrocene/ferrocenium of the ( $\text{Fc}/\text{Fc}^+$ ) redox couple ( $4.8\text{ eV}$  below the vacuum level) was used as the internal calibration. Their HOMO and LUMO energy levels are calculated based on the onset oxidation potential and the onset reduction potential of the redox curves. As shown in Fig. 3, the HOMO and LUMO energy levels of them are  $-4.92$  and  $-3.26\text{ eV}$  for DR3TDTC-C6,  $-4.91$  and  $-3.26\text{ eV}$  for DR3TDTC-C8, respectively. These results are consistent with DR3TDTC's, indicating that carbon-chain isomerism of alkyl chains won't significantly affect the energy level and band gap of molecules. The electrochemical data of DR3TDTC-C6, DR3TDTC-C8 and DR3TDTC are summarized in Table 1.

Table 1

Optical and electrochemical data of DR3TDTC-C6, DR3TDTC-C8 and DR3TDTC [40].

Compound	$\lambda_{\text{max, sol}}$ [nm]	$\epsilon_{\text{sol}}$ [ $\text{M}^{-1}\text{ cm}^{-1}$ ]	$\lambda_{\text{max, film}}$ [nm]	$E_{\text{g}}^{\text{CV}}$ [eV]	HOMO [eV] <sup>a</sup>	LUMO [eV] <sup>a</sup>
DR3TDTC-C6	532	$7.96 \times 10^4$	624	1.66	-4.92	-3.26
DR3TDTC-C8	532	$8.22 \times 10^4$	626	1.65	-4.91	-3.26
DR3TDTC <sup>b</sup>	529	$8.79 \times 10^4$	579	1.66	-4.93	-3.27

<sup>a</sup> As measured by cyclic voltammetry.

<sup>b</sup> Data from Ref. [40].

### 3.3. Photovoltaic properties

BHJ organic solar cells were fabricated using these two molecules as the electron donor materials and  $\text{PC}_{71}\text{BM}$  as the electron acceptor material with a device structure of glass/ITO/PEDOT: PSS/donor: acceptor/ETL-1/Al. The optimum current density vs. voltage ( $J$ - $V$ ) curves measured under AM 1.5G irradiation at an intensity of  $100\text{ mW cm}^{-2}$  are shown in Fig. 4. The external quantum efficiency (EQE) curves of the best devices based on DR3TDTC-C6 and DR3TDTC-C8 are shown in Fig. 5, where the devices with DR3TDTC-C6 and DR3TDTC-C8 exhibit photo-to-current responses from 300 to 800 nm with the maximum EQE value reaching 40% and 41%, respectively. In addition, the device based on DR3TDTC-C8 shows much higher EQE at the wavelength from 563 to 633 nm. Both of their EQE are higher than that of DR3TDTC with value below 15%. It's obvious that among these molecules, linear alkyl chains on the central building block can improve the efficiencies of exciton diffusing and charge transporting.

The device based on DR3TDTC-C6: $\text{PC}_{71}\text{BM}$  without post-treatment shows only a PCE of 0.61%, with open circuit voltage

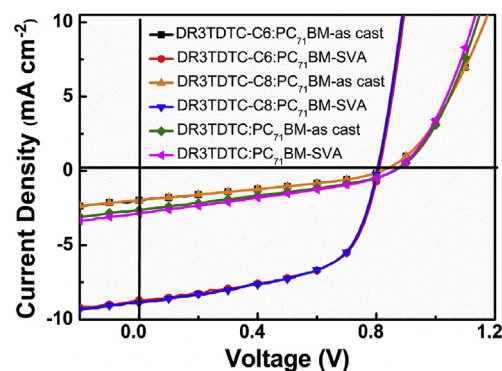


Fig. 4.  $J$ - $V$  curves of DR3TDTC-C6: $\text{PC}_{71}\text{BM}$ , DR3TDTC-C8: $\text{PC}_{71}\text{BM}$  and DR3TDTC: $\text{PC}_{71}\text{BM}$  [40].

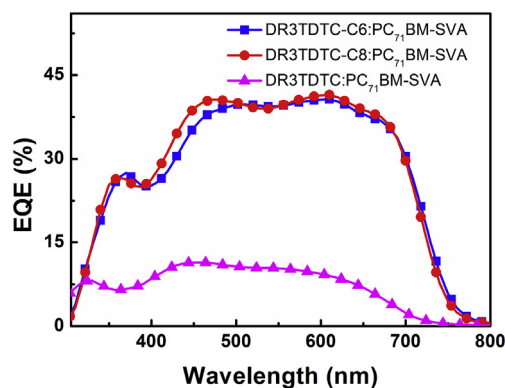


Fig. 5. EQE spectra of DR3TDTC-C6:PC<sub>71</sub>BM, DR3TDTC-C8:PC<sub>71</sub>BM and DR3TDTC:PC<sub>71</sub>BM [40].

( $V_{oc}$ ) of 0.81 V, short circuit current ( $J_{sc}$ ) of  $2.26 \text{ mA cm}^{-2}$ , and fill factor (FF) of 33.3%. There is no surprise to find that the device based on DR3TDTC-C8:PC<sub>71</sub>BM also exhibited a low PCE of 0.52%, with  $V_{oc}$  of 0.819 V,  $J_{sc}$  of  $1.97 \text{ mA cm}^{-2}$ , and FF of 32.1%. All these results are even worse than that of DR3TDTC's [40], the low  $J_{sc}$  and FF of the devices are due to the un-optimized morphologies of the active layers, which can be seen from the transmission electron microscopy (TEM) in the following morphology analysis part. However, unlike DR3TDTC [40], as shown in Table 2, by using solvent vapor annealing (SVA), despite the slight drop of  $V_{oc}$ ,  $J_{sc}$  and FF significantly increased and lead to higher device performance with PCEs of 4.04% for DR3TDTC-C6:PC<sub>71</sub>BM and 4.11% for DR3TDTC-C8:PC<sub>71</sub>BM, respectively.

Compared with DR3TDTC, considering the same central building block and post treatment, the improved  $J_{sc}$  and FF of devices based on these two molecules could be attributed to the influence of linear alkyl side chains attached to the central units. Due to the lower steric hindrance, the solvent molecules inside the BHJ thin film can promote crystallization and aggregation of donor materials during the process of solvent vapor annealing [44]. We also tried to use thermal annealing to improve the film morphology, but unfortunately, only resulted in even larger domains and thus worse performance.

### 3.4. Light absorption and charge transport property

To further understand the relatively better performance of the DR3TDTC-C6 and DR3TDTC-C8 based devices, the absorption and charge transport properties of the blend films were investigated. As shown in Fig. 6, compared with the DR3TDTC:PC<sub>71</sub>BM blend films, the DR3TDTC-C6:PC<sub>71</sub>BM and DR3TDTC-C8:PC<sub>71</sub>BM blend films with and without SVA all show red-shifted absorption. However,

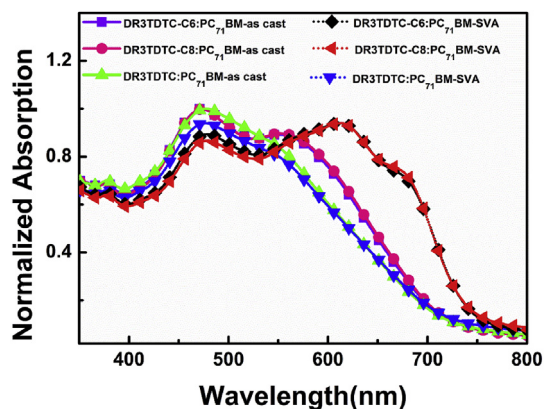


Fig. 6. UV-vis absorption spectra of as cast and solvent vapor annealing blend films of DR3TDTC-C6:PC<sub>71</sub>BM, DR3TDTC-C8:PC<sub>71</sub>BM and DR3TDTC:PC<sub>71</sub>BM [40].

the blend films of DR3TDTC exhibit much blue-shifted absorption peak compared with the pure donor films (see Fig. 2 and Table 1), but the blend films of DR3TDTC-C6 and DR3TDTC-C8 didn't show similar phenomenon, indicating that the addition of PC<sub>71</sub>BM has weak impact on intermolecular packing of DR3TDTC-C6 and DR3TDTC-C8. After SVA treatment, the absorption peak of DR3TDTC-C6:PC<sub>71</sub>BM and DR3TDTC-C8:PC<sub>71</sub>BM blend films is red-shifted about 50 nm. However, the blend films of DR3TDTC:PC<sub>71</sub>BM remain unchanged. And after SVA, the absorption peak of DR3TDTC-C6:PC<sub>71</sub>BM and DR3TDTC-C8:PC<sub>71</sub>BM blend films all exhibit an increasing shoulder peak at about 680 nm. These results suggest that better molecular packing is formed for DR3TDTC-C6 and DR3TDTC-C8 after SVA treatment [45–48].

The hole mobilities of these molecules were measured by the space charge limited current (SCLC) method (see Fig. S2, Fig. S3). For the devices without any treatment, the hole mobilities are  $5.18 \times 10^{-5} \text{ cm}^2 \text{ V}^{-1} \text{ s}^{-1}$  for the DR3TDTC-C6 blend film and  $6.55 \times 10^{-5} \text{ cm}^2 \text{ V}^{-1} \text{ s}^{-1}$  for the DR3TDTC-C8 blend film, respectively. After SVA treatment, the hole mobilities are improved to  $5.28 \times 10^{-4} \text{ cm}^2 \text{ V}^{-1} \text{ s}^{-1}$  for the DR3TDTC-C6 blend film and  $6.02 \times 10^{-4} \text{ cm}^2 \text{ V}^{-1} \text{ s}^{-1}$  for the DR3TDTC-C8 blend film, respectively. For the devices without any treatment, the electron mobilities are  $5.88 \times 10^{-5} \text{ cm}^2 \text{ V}^{-1} \text{ s}^{-1}$  for the DR3TDTC-C6 blend film and  $6.56 \times 10^{-5} \text{ cm}^2 \text{ V}^{-1} \text{ s}^{-1}$  for the DR3TDTC-C8 blend film, respectively. After SVA treatment, the electron mobility increases significantly to  $1.47 \times 10^{-4} \text{ cm}^2 \text{ V}^{-1} \text{ s}^{-1}$  for the DR3TDTC-C6 blend film, and the mobility for the DR3TDTC-C8 blend film is  $1.67 \times 10^{-4} \text{ cm}^2 \text{ V}^{-1} \text{ s}^{-1}$ . After SVA treatment, these two new molecules show much improved and more balanced hole and electron mobilities than the data of DR3TDTC based blend films.

### 3.5. Film microstructure and morphology analysis

To further investigate the influence of alkyl chains on intermolecular packing at solid state, the microstructures of the films were characterized by grazing-incidence wide-angle X-ray scattering (GIWAXS). As shown in Fig. 7, DR3TDTC-C6:PC<sub>71</sub>BM and DR3TDTC-C8:PC<sub>71</sub>BM blend films without post treatment showed neither (010) reflection nor multiple higher-order (h00) reflections along the  $q_z$ -direction. Along  $q_{xy}$ -direction, both of the films showed (100) reflection at  $0.33 \text{ \AA}^{-1}$ , corresponding to an inter-chain distance of  $19.0 \text{ \AA}$ . After SVA, both of them showed (010) reflection as well as multiple higher-order (h00) reflections along two directions, the positions of (010) reflections were  $1.70 \text{ \AA}^{-1}$ , corresponding to  $\pi$ - $\pi$  stacking distances of  $3.69 \text{ \AA}$ . Besides, the peaks of (h00) reflections is much more intensive than that of (010)

Table 2

Photovoltaic characteristics of the OPV devices based on DR3TDTC-C6, DR3TDTC-C8 and DR3TDTC [40].

Donor	$V_{oc}$ [V] <sup>c</sup>	$J_{sc}$ [ $\text{mA cm}^{-2}$ ] <sup>c</sup>	FF <sup>c</sup>	PCE [%] <sup>c</sup>
DR3TDTC-C6 <sup>a</sup>	0.81	1.99	0.32	0.51
DR3TDTC-C6 <sup>b</sup>	0.80	8.70	0.57	4.04
DR3TDTC-C8 <sup>a</sup>	0.81	1.97	0.32	0.51
DR3TDTC-C8 <sup>b</sup>	0.80	8.86	0.58	4.11
DR3TDTC <sup>a,d</sup>	0.86	2.63	0.32	0.72
DR3TDTC <sup>b,d</sup>	0.85	2.85	0.31	0.75

<sup>a</sup> Without post treatment.

<sup>b</sup> With SVA treatment: CF 90s.

<sup>c</sup> Average value from 20 devices.

<sup>d</sup> Data from Ref. [40].

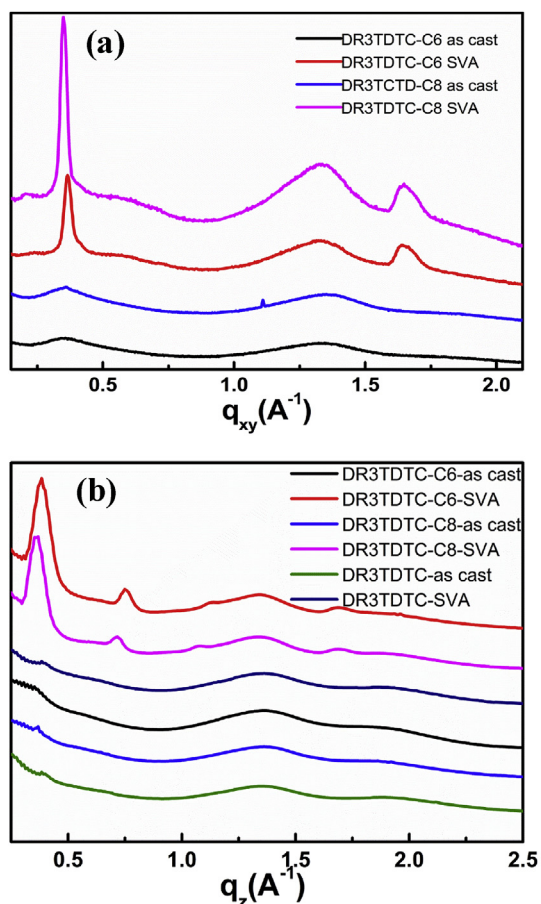


**Fig. 7.** (a) In-plane and (b) Out-of-plane line cut profiles of as cast and solvent vapor annealing blend films of DR3TDTC-C6: PC<sub>71</sub>BM, DR3TDTC-C8: PC<sub>71</sub>BM and DR3TDTC: PC<sub>71</sub>BM [40].

reflections along these two directions. But For DR3TDTC:PC<sub>71</sub>BM blend films, even after SVA treatment, there was still no (010) reflection appeared [40], which indicates that among these three molecules, only molecules with linear alkyl chains on core units can form favorable long-range order and crystallinity for better charge transport, which is consistent with their higher  $J_{sc}$  and FF.

Resonant soft X-ray scattering (RSoXS) were also taken to investigate the phase separation of the blend films. As shown in Fig. 8, the DR3TDTC-C6:PC<sub>71</sub>BM blend films with SVA treatment show an interference at  $q = 0.00787 \text{ \AA}^{-1}$ , ( $q$  is the scattering

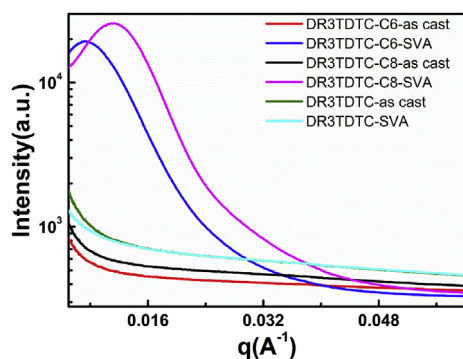


**Fig. 8.** RSoXS profiles of as cast and solvent vapor annealing blend films of DR3TDTC-C6:PC<sub>71</sub>BM, DR3TDTC-C8:PC<sub>71</sub>BM and DR3TDTC:PC<sub>71</sub>BM [40].

vector), corresponding to a domain center-to-center distance of 79.8 nm. For DR3TDTC-C8:PC<sub>71</sub>BM with SVA treatment, an interference at  $q = 0.01124 \text{ \AA}^{-1}$  is observed, corresponding to a shorter domain center-to-center distance of 55.9 nm. However, DR3TDTC:PC<sub>71</sub>BM without (and with) SVA, no significant interference is observed, indicating no clear phase separation in these blend films.

Transmission electron microscopy (TEM) studies (Fig. 9) showed that before annealing, both DR3TDTC-C6:PC<sub>71</sub>BM and DR3TDTC-C8:PC<sub>71</sub>BM blend films show no obvious phase separation of the donor and acceptor, which could be unfavorable for charge transport, thus leading to low  $J_{sc}$  and FF. Similar case was observed for DR3TDTC:PC<sub>71</sub>BM devices [40]. After SVA treatment, the DR3TDTC:PC<sub>71</sub>BM blend film still show no clear phase separation, this could be due to the poor packing properties of DR3TDTC. However, for DR3TDTC-C6:PC<sub>71</sub>BM and DR3TDTC-C8:PC<sub>71</sub>BM devices with SVA treatment, the films exhibited homogeneous interpenetrating network with a domain size of ~60 nm, the better morphologies of DR3TDTC-C6:PC<sub>71</sub>BM and DR3TDTC-C8:PC<sub>71</sub>BM blend films with SVA could increase exciton dissociation and charge transport efficiency and reduce charge carriers recombination. In addition, compared with DR3TDTC-C8, DR3TDTC-C6 owns shorter alkyl chains, which might help it packed more compactly, and forms a larger domain. The TEM result (Fig. 9) is consistent with

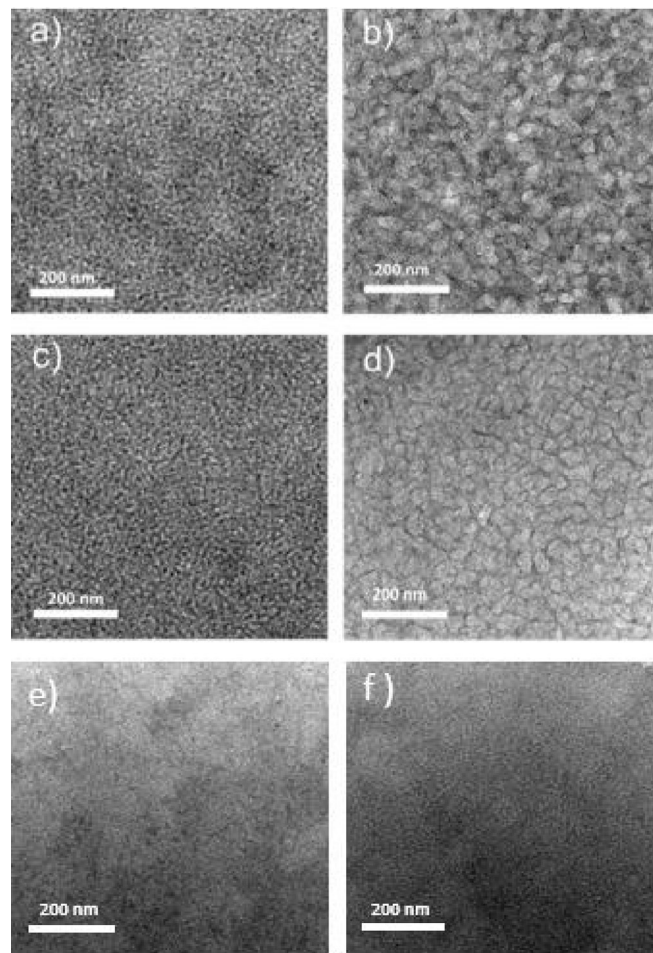


**Fig. 9.** TEM images of (a, b) DR3TDTC-C6:PC<sub>71</sub>BM (1:0.8, w/w), (c, d) DR3TDTC-C8:PC<sub>71</sub>BM (1:0.8, w/w) and (e, f) DR3TDTC:PC<sub>71</sub>BM (1:0.8, w/w) blend films [40]. (Panels a, c, e show the blend films without post-treatment; panels b, d, f shows the blend films with SVA treatment.)

that from the RSoXS analysis.

The remarkably difference in morphology and device performance of the three molecules must be attributed to the change of alkyl chains on the central building block. Compared to DR3TDTC, the linear alkyl chains on the donor unit of DR3TDTC-C6 and DR3TDTC-C8 could reduce the steric hindrance caused by bulky branched alkyl chains, which led to stronger  $\pi$ - $\pi$  interactions between the molecule backbones. The more compact packing of DR3TDTC-C6 and DR3TDTC-C8 at solid state could provide better optical absorption, higher mobility, and better phase separation than that of DR3TDTC. Therefore, the devices based on DR3TDTC-C6 and DR3TDTC-C8 promote the photovoltaic performance from DR3TDTC's poor PCE of <1% to PCEs over 4%.

#### 4. Conclusions

In conclusion, we synthesized two small molecule donors named DR3TDTC-C6 and DR3TDTC-C8 with n-hexyl and n-octyl alkyl chains on the central building block DTC. The influences of the alkyl chains on properties of small molecule were systematically investigated. Although there is only a little change on the central unit compared to the molecule DR3TDTC, these two new molecules showed significant different properties such as film absorption, molecular packing and charge transport in contrast with that of DR3TDTC. Devices based on these two molecules with linear alkyl chains show noticeable improvement in  $J_{sc}$  and FF after SVA treatment. The result demonstrated a good example of the significant effects of alkyl side chains on the molecules physical properties and photovoltaic performances, which will give valuable lessons on the future high efficiency molecule design.

#### Acknowledgement

The authors gratefully acknowledge the financial support from MOST (2014CB643502, 2016YFA0200200) and NSF (91433101, 51422304, 51373078) of China.

#### Appendix A. Supplementary data

Supplementary data related to this article can be found at <http://dx.doi.org/10.1016/j.dyepig.2017.02.015>.

#### References

- [1] Arias AC, MacKenzie JD, McCulloch I, Rivnay J, Salleo A. *Chem Rev* 2010;110:3.
- [2] Chen L-M, Hong Z, Li G, Yang Y. *Adv Mater* 2009;21:1434.
- [3] Giroto C, Cheyng D, Aernouts T, Banishoeib F, Lutsen L, Cleij TJ, et al. *Org Electron* 2008;9:740.
- [4] Heeger AJ. *Chem Soc Rev* 2010;39:2354.
- [5] Krebs FC. *Sol Energy Mater Sol Cells* 2009;93:394.
- [6] Lin Y, Dam HF, Andersen TR, Bundgaard E, Fu W, Chen H, et al. *J Mater Chem C* 2013;1:8007.
- [7] Lipomi DJ, Bao Z. *Energy Environ Sci* 2011;4:3314.
- [8] Po R, Maggini M, Camaioni N. *J Phys Chem C* 2010;114:695.
- [9] Chen J-D, Cui C, Li Y-Q, Zhou L, Ou Q-D, Li C, et al. *Adv Mater* 2015;27:1035.
- [10] He Z, Zhong C, Su S, Xu M, Wu H, Cao Y. *Nat Phot* 2012;6:591.
- [11] Kong J, Hwang I-W, Lee K. *Adv Mater* 2014;26:6274.
- [12] Li C-Z, Chang C-Y, Zang Y, Ju H-X, Chueh C-C, Liang P-W, et al. *Adv Mater* 2014;26:6262.
- [13] Liao S-H, Jhuo H-J, Cheng Y-S, Chen S-A. *Adv Mater* 2013;25:4766.
- [14] Ye L, Zhang S, Zhao W, Yao H, Hou J. *Chem Mater* 2014;26:3603.
- [15] Liu Y, Zhao J, Li Z, Mu C, Ma W, Hu H, et al. *Nat Commun* 2014;5.
- [16] Vohra V, Kawashima K, Kakara T, Koganezawa T, Osaka I, Takimiya K, et al. *Nat Photonics* 2015;9:403.
- [17] Huang J, Carpenter JH, Li C-Z, Yu J-S, Ade H, Jen AKY. *Adv Mater* 2016;28:967.
- [18] Zhang S, Ye L, Zhao W, Yang B, Wang Q, Hou J. *Sci China Chem* 2015;58:248.
- [19] Liu T, Huo L, Sun X, Fan B, Cai Y, Kim T, et al. *Adv Energy Mater* 2016;6 [n/a].
- [20] Hu H, Jiang K, Yang G, Liu J, Li Z, Lin H, et al. *J Am Chem Soc* 2015;137:14149.
- [21] Zheng Z, Zhang S, Zhang J, Qin Y, Li W, Yu R, et al. *Adv Mater* 2016;28:5133.
- [22] Gupta V, Kyaw AKK, Wang DH, Chand S, Bazan GC, Heeger AJ. *Sci Rep* 2013;3:1965.
- [23] Kan B, Zhang Q, Li M, Wan X, Ni W, Long G, et al. *J Am Chem Soc* 2014;136:15529.
- [24] Zhang H, Ye L, Hou J. *Polym Int* 2015;64:957.
- [25] Li M, Gao K, Wan X, Zhang Q, Kan B, Xia R, et al. *Nat Photonics* 2017;11:85–90.
- [26] Lan S-C, Raghunath P, Lu Y-H, Wang Y-C, Lin S-W, Liu C-M, et al. *ACS Appl Mater Interfaces* 2014;6:9298.
- [27] Ni W, Wan X, Li M, Wang Y, Chen Y. *Chem Commun* 2015;51:4936.
- [28] Qin H, Li L, Guo F, Su S, Peng J, Cao Y, et al. *Energy Environ Sci* 2014;7:1397.
- [29] Walker B, Kim C, Nguyen T-Q. *Chem Mater* 2011;23:470.
- [30] Chen C, Cheng M, Liu P, Gao J, Kloo L, Sun L. *Nano Energy* 2016;23:40.
- [31] Chiu S-W, Lin L-Y, Lin H-W, Chen Y-H, Huang Z-Y, Lin Y-T, et al. *Chem Commun* 2012;48:1857.
- [32] Fitzner R, Mena-Osteritz E, Walzer K, Pfeiffer M, Bäuerle P. *Adv Funct Mater* 2015;25:1845.
- [33] Mishra A, Popovic D, Vogt A, Kast H, Leitner T, Walzer K, et al. *Adv Mater* 2014;26:7217.
- [34] Patra D, Huang T-Y, Chiang C-C, Maturana ROV, Pao C-W, Ho K-C, et al. *ACS Appl Mater Interfaces* 2013;5:9494.
- [35] Shen S, Jiang P, He C, Zhang J, Shen P, Zhang Y, et al. *Chem Mater* 2013;25:2274.
- [36] Ni W, Li M, Wan X, Zuo Y, Kan B, Feng H, et al. *Sci China Chem* 2015;58:339.
- [37] Kim K-H, Yu H, Kang H, Kang DJ, Cho C-H, Cho H-H, et al. *J Mater Chem A* 2013;1:14538.
- [38] Liu Y, Wan X, Wang F, Zhou J, Long G, Tian J, et al. *Adv Energy Mater* 2011;1:771.
- [39] Lan S-C, Chang C-K, Lu Y-H, Lin S-W, Jen AKY, Wei K-H. *RSC Adv* 2015;5:67718.
- [40] Ni W, Li M, Liu F, Wan X, Feng H, Kan B, et al. *Chem Mater* 2015;27:6077–84.
- [41] Li C-Z, Chueh C-C, Yip H-L, O'Malley KM, Chen W-C, Jen AKY. *J Mater Chem* 2012;22:8574.
- [42] Bijleveld JC, Shahid M, Gilot J, Wienk MM, Janssen RAJ. *Adv Funct Mater* 2009;19:3262.
- [43] Helgesen M, Krebs FC. *Macromolecules* 2010;43:1253.
- [44] Li M, Liu F, Wan X, Ni W, Kan B, Feng H, et al. *Adv Mater* 2015;27:6296.
- [45] Chen H, Hsiao Y-C, Hu B, Dadmun M. *J Mater Chem A* 2014;2:9883.
- [46] Liao HC, Tsao CS, Huang YC, Jao MH, Tien KY, Chuang CM, et al. *RSC Adv* 2014;4:6246.
- [47] Verploegen E, Miller CE, Schmidt K, Bao Z, Toney MF. *Chem Mater* 2012;24:3923.
- [48] Viterisi A, Gispert-Guirado F, Ryan JW, Palomares E. *J Mater Chem* 2012;22:15175.